INFECTION AND IMMUNITY, Aug. 2008, p. 3491–3501 Vol. 76, No. 8
0019-9567/08/$08.00+0 doi:10.1128/IAI.00254-08

Temporal and Spatial Distribution of *Toxoplasma gondii* Differentiation into Bradyzoites and Tissue Cyst Formation In Vivo▽

Manlio Di Cristina,[1] Daniela Marocco,[1] Roberto Galizi,[1] Carla Proietti,[1] Roberta Spaccapelo,[1] and Andrea Crisanti[1,2]*

Department of Experimental Medicine and Biochemical Sciences, University of Perugia, Via Del Giochetto, 06122 Perugia, Italy,[1] *and Division of Molecular and Cell Biology, Imperial College, Imperial College Road, London SW7 2AZ, United Kingdom*[2]

Received 22 February 2008/Returned for modification 31 March 2008/Accepted 15 May 2008

During *Toxoplasma gondii* infection, a fraction of the multiplying parasites, the tachyzoites, converts into bradyzoites, a dormant stage, which form tissue cysts localized mainly in brain, heart, and skeletal muscles that persist for several years after infection. At this stage the parasite is protected from the immune system, and it is believed to be inaccessible to drugs. While the long persistence of tissue cysts does not represent a medical problem for healthy individuals, this condition represents a major risk for patients with a compromised immune system, who can develop recrudescent life-threatening *T. gondii* infections. We have investigated for the first time the dynamics and the kinetics of tachyzoite-to-bradyzoite interconversion and cyst formation in vivo by using stage-specific bioluminescent parasites in a mouse model. Our findings provide a new framework for understanding the process of bradyzoite differentiation in vivo. We have also demonstrated that complex molecules such as D-luciferin have access to tissue cysts and are metabolically processed, thus providing a rationale for developing drugs that attack the parasite at this developmental stage.

Toxoplasma gondii is transmitted to humans by the ingestion of either undercooked meat containing tissue cysts or poorly washed vegetables contaminated with oocysts from cat feces. The infection normally progresses as a mild, self-resolving disease. Initially *T. gondii* multiplies rapidly inside cells of different tissues and organs in the form of tachyzoites. Within 2 to 3 weeks, infected individuals develop a potent immune response that effectively controls the growth of the parasite. Before being eliminated by the immune system, some of the tachyzoites develop into a dormant stage, the bradyzoites, which multiply at a much lower rate than tachyzoites and become progressively enclosed in a dense matrix surrounded by a thick wall, the tissue cyst (11, 33, 46). At this stage the parasite is much less vulnerable to attack by the immune system. Tissue cysts can persist for several years in the brain, the heart, and the skeletal muscle of individuals who had been previously infected with *T. gondii* (34, 46, 49). Tissue cysts do not cause major pathological damage, and parasites are eventually released as result of stochastic reactivation of the bradyzoites (14) yet are promptly eliminated by the immune system. Therefore, in healthy individuals the persistence of *T. gondii* cysts in tissues and organs does not represent a cause for concern. However, several conditions may appear later in life that impair the function of the immune system and its ability to control the reactivation of *T. gondii* tissue cysts. These include infectious diseases such as human immunodeficiency virus infection (28–30) and treatment with immunosuppressive and chemotherapeutic agents commonly given to transplant and cancer patients, respectively (3, 18, 22, 27, 32, 45). Reactivation of tissue cysts in these individuals leads to the recrudescence of *T. gondii* infection (15), a life-threatening condition that in the long term responds poorly to therapy and often develops into encephalitis (16, 19, 26, 28, 30, 42). The persistence of tissue cysts therefore represents a problem of great medical relevance given the increasing number of people under immunosuppressive and antitumor therapy and the prevalence of individuals with dormant *T. gondii*, which in some cases can be as high as 80% of the adult population.

The factors that trigger the conversion of tachyzoites to bradyzoites in vivo and the molecular events that lead to cyst formation and reactivation are poorly understood. Immune-derived factors produced in response to the infection, such as gamma interferon, tumor necrosis factor alpha, and nitric oxide, have been suggested to play a role in triggering the differentiation of tachyzoites into bradyzoites and progress to cyst formation (6, 7, 31, 37). Under in vitro culture conditions, tachyzoites can be induced to differentiate into bradyzoites after exposure to alkaline pH (39, 47) or by other stimuli such as sodium nitroprusside and inhibitors of cyclic nucleotide kinases (7, 12, 24, 38). The cyst is believed to protect the parasite from the host immune system and act as a barrier for antiparasitic compounds. The general consensus is that tissue cysts are resistant to drugs commonly used to treat *Toxoplasma* infection, including pyrimethamine, sulfadiazine, and atovaquone, either alone or in combination (1, 2, 13, 15, 17, 21, 25, 44).

We exploited knowledge on promoters transcribed in the bradyzoite and on bioluminescent technology to develop an in vivo system for analyzing the temporal and spatial distribution of tachyzoite-to-bradyzoite differentiation and cyst formation. Monitoring bradyzoite differentiation and cyst formation in vivo is anticipated to expand our knowledge on this crucial aspect of the biology of the parasite and at the same time will

* Corresponding author. Mailing address: Division of Molecular and Cell Biology, Imperial College, Imperial College Road, London SW7 2AZ, United Kingdom. Phone: 44 207 5945426. Fax: 44 207 5945439. E-mail: acrs@imperial.ac.uk.

▽ Published ahead of print on 27 May 2008.

provide a readout system to assess the activity of compounds targeting the parasite at this developmental stage.

MATERIALS AND METHODS

Host cells and parasite cultures. Human foreskin fibroblast (HFF) and Vero cells were grown in Dulbecco's modified Eagle medium (Invitrogen) containing 10% fetal bovine serum (Invitrogen). A single *T. gondii* line, the clonal isolate PLK of the ME49 strain, was used in all genetic manipulations described here. The parasites were propagated in vitro by serial passage on monolayers of HFF or Vero cells (35). In vitro tachyzoite-to-bradyzoite conversion was induced by exposing parasite cultures to pH 8.1 as described previously (39, 47). Briefly, bradyzoite differentiation was induced in vitro by culturing tachyzoite-infected cells in RPMI 1640 buffered with 50 mM HEPES to pH 8.1, in absence of CO_2, and supplemented with 1% fetal bovine serum.

Transformation vectors. *T. gondii* tachyzoites were transformed using expression vectors generated from the basic plasmid pBluescript II SK1 (Stratagene). The plasmid pSRS9/F-Luc was designed to contain the putative promoter sequence of the *SRS9* gene spanning 1,470 nucleotides upstream of its start codon followed by the coding sequence of the firefly luciferase gene (*F-Luc*) and the 3′ untranslated region (3′UTR) from the *GRA1* gene, consisting of 414 nucleotides downstream of the stop codon. The *SRS9* promoter was amplified by PCR from *T. gondii* genomic DNA (strain PLK) using the forward primer MDC1 (5′-GGG GCT GCA GTG TCA CCG GTT CGG TGC ACT-3′) and the reverse primer MDC2 (5′-GTC AAA GCT TCA GAT CTG GCG CGC CTG TGT CGA CCC GTG TGC ACG GTT CCT-3′) containing the target sequence of the PstI and HindIII endonucleases to direct cloning into the plasmid pBluescript II SK1. The sequence encompassing the 3′UTR of the *GRA1* gene was obtained in PCR experiments using as the template genomic DNA of PLK parasites with the forward primer MDC3 (5′-GGG AAG CTT GAC TAC GAC GAA AGT GAT GCG CAG GC-3′) and the reverse primer MDC4 (5′-AAT GCT CGA GTG GAA CTA CGG TGT TTG TTC CTT TC-3′). The PCR product was cloned between the HindIII and XhoI sites downstream of the *SRS9* promoter. The sequence carrying the *F-Luc* was amplified by PCR from the vector pL0028, obtained from the Malaria Research and Reference Reagent Resource Center (http://www.malaria.mr4.org/), using the forward primer MDC5 (5′-CCC CGT CGA CAC AAT GGA AGA CGC CAA AAA CAT AAA G-3′) and the reverse primer MDC6 (5′-CCC AAG CTT ACA CGG CGA TCT TTC CGC CCT TCT TG-3′). To generate the construct pSRS9/F-Luc, the F-Luc sequence was cloned between the *SRS9* promoter and the *GRA1* 3′UTR using the SalI and HindIII sites (Fig. 1). To generate pSRS9/EGFP-SAG1/R-Luc, the sequence encoding enhanced green fluorescent protein (EGFP) was amplified from pMyc/EGFP (provided by Furio Spano) using the forward primer MDC10 (5′-CCC CGT CGA CAC AAT GAG TAA AGG AGA AGA ACT TTT CAC TGG AGT TGT CCC AAT T-3′) and the reverse primer MDC11 (5′-GGG GAA GCT TAT TTG TAT AGT TCA TCC ATG CCA TGT G-3′) and cloned in the SalI and HindIII sites of pSRS9/F-Luc, thereby swapping the *F-Luc* gene with the EGFP sequence and generating the intermediate vector pSRS9/EGFP. This construct was used to insert the expression cassette SAG1promoter/R-Luc/SAG1-3′UTR. This was generated by amplifying the coding sequence of the *Renilla* luciferase gene (*R-Luc*) from the pGL4.75[hRluc/CMV] vector (Promega) using the forward primer MDC80 (5′-CCC CAT GCA TTC CAA GGT GTA CGA CCC CGA GCA ACG C-3′) and the reverse primer MDC81 (5′-CCC CTT AAT TAA TTA CTG CTC GTT CTT CAG CAC GCG C-3′). The PCR product was cloned into the NsiI and PacI sites of pSAG1/2-CAT (40). The expression cassette SAG1promoter/R-Luc/SAG1-3′UTR was then cut out using the XhoI and XbaI restriction enzymes and, after blunting the XhoI end by T4 DNA polymerase treatment, cloned between the SmaI and XbaI sites upstream of the *SRS9* promoter of the vector pSRS9/EGFP. The expression vector pSRS9/EGFP-BAG1/F-Luc, in which *F-Luc* is under the control of the *BAG1* promoter, was generated following the same cloning scheme used to generate pSRS9/EGFP-SAG1/R-Luc. Briefly, the PstI/SalI fragment encompassing the *SRS9* promoter of pSRS9/F-Luc was replaced with the sequence containing the *BAG1* promoter to generate pBAG1/F-Luc. From the latter, an XbaI/XhoI fragment was excised and cloned between SmaI and XbaI sites in pSRS9/EGFP to generate pSRS9/EGFP-BAG1/F-Luc. The sequence encompassing the *BAG1* promoter was obtained by PCR amplification from genomic *Toxoplasma* DNA with the forward primer MDC69 (5′-AAT CCT GCA GCC AGT TGC CCG GCT CTG GGT ACC TTC TTC TCG-3′) and the reverse primer MDC71 (5′-AAC CCT CGA GAT ATC ATA CGG GAC CTG GGC TTT GCA G-3′). pBAG1/EGFP was generated by swapping the *SRS9* promoter with that of the *BAG1* gene.

All constructs were sequenced to rule out the occurrence of nucleotide substitutions in either the promoter or the coding sequences.

Genetic manipulation of parasites. To insert *F-Luc* under the transcriptional control of the *SRS9* promoter in *T. gondii*, extracellular tachyzoites were transformed using the constructs pSRS9/F-Luc and pT/230-CAT. The latter contains the selectable chloramphenicol acetyltransferase marker (23, 40). In these experiments, 2×10^7 freshly harvested tachyzoites were resuspended in 700 μl of cytomix (23) containing 100 μg of pSRS9/F-Luc, 10 μg of pT/230, and 100 U of NotI. Prior to electroporation, the two plasmids were linearized with the endonuclease NotI (5) and mixed in a 10:1 mass ratio. Electroporated parasites were subjected to chloramphenicol selection as described previously (23). After 7 to 10 days, stable populations of parasites resistant to chloramphenicol emerged. Individual clones were isolated by limiting dilution. Parasite clones carrying both pT/230-CAT and pSRS9/F-Luc were subsequently transformed with the construct combination of pSRS9/EGFP-SAG1/R-Luc and pT/230-Bleo to introduce the EGFP and *R-Luc* genes under the control of bradyzoite (*SRS9*)- and tachyzoite (*SAG1*)-transcribed promoters, respectively. Transformation was carried out as described above, recombinant parasites were selected by exposing extracellular tachyzoites to three rounds of 12 h of incubation with phleomycin at 10 μg/ml (Sigma) (41), and individual clones were isolated by limiting dilution. The H3 clone carrying both pSRS9/F-Luc and pT/230-CAT was also subsequently transformed with the constructs pBAG1/EGFP and pT/230-Bleo to generate parasites expressing the *F-Luc* and EGFP genes under control of the *SRS9* and *BAG1* promoters, respectively. Single clones of *Toxoplasma* expressing the *F-Luc* and EGFP genes under the control of the *BAG1* and *SRS9* promoters, respectively, were obtained by cotransforming wild-type PLK tachyzoites with the two NotI-linearized plasmids, pSRS9/EGFP-BAG1/F-Luc and pT/230-CAT.

Expression analysis of bradyzoite markers. Mice were infected with 10^6 H3F33 tachyzoites by intraperitoneal (i.p.) injection and after 5 days were analyzed for *F-Luc* activity by bioluminescence imaging (BLI). Positive mice were culled, and parasites were recovered from the i.p. cavity by phosphate-buffered saline (PBS) lavage. Total RNA was extracted from parasites using the RNeasy minikit (Qiagen), and 1 μg of RNA was reverse transcribed using the SuperScript III first-strand synthesis system for reverse transcription-PCR (RT-PCR) (Invitrogen) and used as the template for each PCR (35 cycles of 95°C for 30 s, 60°C for 30 s, and 72°C for 60 s). PCRs were performed in 20 μl, and the whole reaction products were loaded on a 1% agarose gel. The primers to reveal the transcription of bradyzoite specific genes were as follows: *BAG1*, forward primer MDC135 (5′-CGA TGA TCT CAG AAA TAG GCT GAG TCA CGA C-3′) and reverse primer MDC136 (5′-CCT CGA CCT TGA TCG TGA CAC GTA GAA CGC CG-3′); *ENO1*, forward primer MDC169 (5′-GTT ATC AAG GAC ATC GTT GCA CGC GAG ATT TTG-3′) and reverse primer MDC170 (5′-ATT CAG AGC CTC TTC AGC AGT GGC TAC-3′); *ENO2*, forward primer MDC167 (5′-GCC ATC AAG GAC ATC ACT GCT CGT CAG ATC CTC-3′) and reverse primer MDC171 (5′-CTT GCG TTG CGA CTT GTC GTT GTT CGG AGT C-3′); *LDH1*, forward primer MDC211 (5′-GCA CGT GTA CGC AAG ACA GCT TCG CAG AC-3′) and reverse primer MDC213 (5′-GTA AGA GTA CTC AGC ACG G −3′); *LDH2*, forward primer MDC207 (5′-CTT TGC GCT GCT CGG CAT TCG TAC TTC AC-3′) and reverse primer MDC209 (5′-TCA TAC TGG TTT GCG CTC GTC-3′); and *PMA1*, forward primer MDC202 (5′-CGA CAC ACG AGG CCT GAC GTC GGA CCA AG-3′) and reverse primer MDC201 (5′-CGC GCA TGT TGT CCT CCA CCA CGC AGA CTG-3′). Primer pairs for all selected genes flanked an intron within the genomic sequence which allowed the discrimination of PCR products obtained from cDNA versus genomic DNA.

Animal studies. Female C57BL/6 mice (5 weeks old; Charles River) and Swiss-CD1 mice (5 weeks old; Harlan Sprague-Dawley) were inoculated with either wild-type or transgenic parasites by i.p. injection. To maximize parasite viability, the mice were infected with freshly purified tachyzoites isolated from scraped infected HFF cells by passage through a 27-gauge needle. Oral infection of mice was carried out by gavage using brain homogenate containing tissue cysts.

Cyst purification. Mouse brains were harvested at 10 to 20 days postinfection and homogenized in 2 ml of PBS by syringe passage through a 19-gauge needle. The average cyst number was determined by counting four samples (100 μl each) of brain homogenate under inverted fluorescence microscopy. Cysts were purified from brain by isopycnic centrifugation as previously described (9, 48). Release of bradyzoites from purified cysts was carried out by incubating purified cysts in 0.5% trypsin (1:250) for 5 min at 37°C.

BLI analysis. BLIs were captured using an intensified-charge-coupled device photon-counting video camera from an in vivo imaging system (IVIS200; Xenogen) and processed using the software LIVING IMAGE 2.50.1 and IGOR PRO 4.09A (Xenogen). In vitro BLI analysis of transgenic parasites was performed using freshly purified extracellular parasites in the presence of either 0.15 mg/ml of D-luciferin (Xenogen, Alameda, CA) or 10 μg/ml of coelenterazine (Nanolight), the substrates of firefly and *Renilla* luciferases, respectively. Upon addition

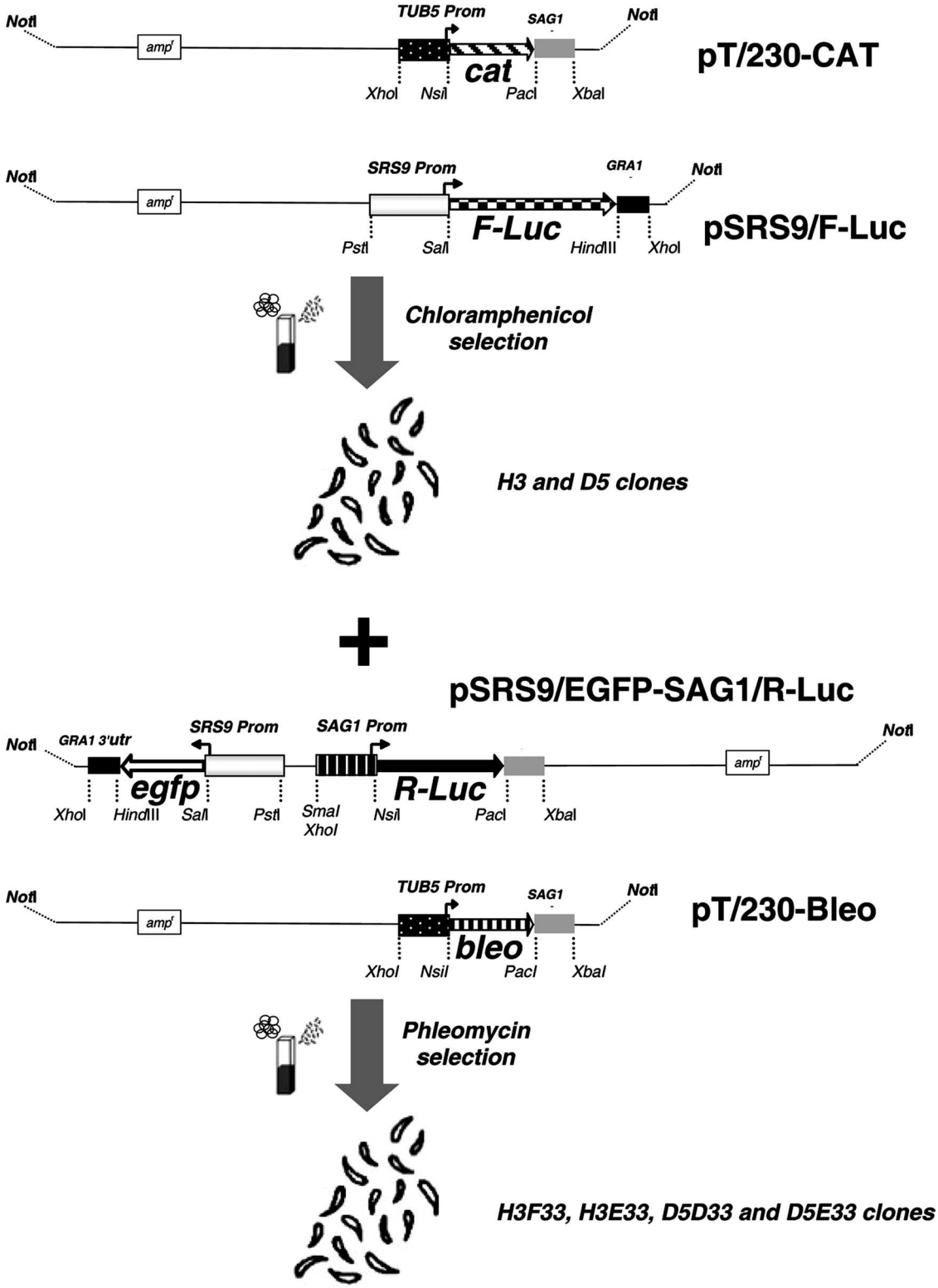

FIG. 1. Generation of transgenic *Toxoplasma* lines. A schematic representation of the constructs developed and the strategy employed to generate *T. gondii* stage-specific bioluminescent lines is shown. The parasites were first transformed with a mixture of two plasmids: (i) pT/230-CAT, providing the selectable chloramphenicol acetyltransferase marker (hatched arrow) under control of the tubulin 5 (*TUB5*) promoter (black box), and (ii) pSRS9/F-Luc, containing the *F-Luc* gene (striped arrow) under transcriptional control of the bradyzoite transcribed *SRS9* promoter (white box). Clones H3 and D5 were further utilized for a second transformation step using two additional constructs: (i) PT/230-Bleo, providing a second selectable marker, *Bleo* (striped arrow), under control of the *TUB5* promoter, and (ii) pSRS9/EGFP-SAG1-R-Luc, containing the EGFP-coding sequence (white arrow) and the *R-Luc* gene (black arrow) under the transcriptional control of the *SRS9* (white box) and *SAG1* (black box) promoters, respectively.

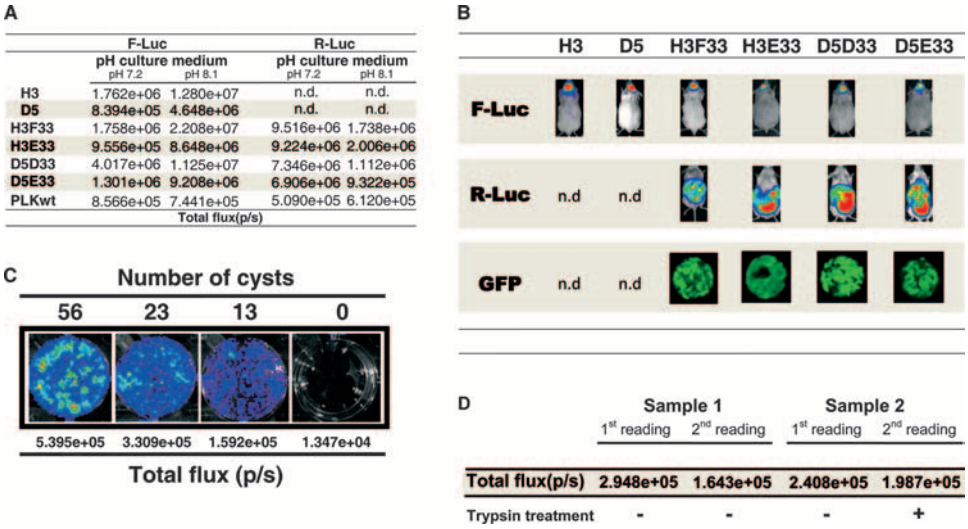

FIG. 2. Phenotypic analysis of transgenic parasites at different developmental stages. (A) Expression of *F-Luc* and *R-Luc* in cultured parasites. The clones H3, D5, H3F33, H3E33, D5D33, and D5E33 were cultured on HFF cells either under standard conditions (pH 7.2) or with exposure to alkaline medium (pH 8.1) to induce tachyzoite switching to bradyzoites. As control, the parental line PLK was also treated in the same way. The numbers represent photon emission fluxes collected from samples containing equal amounts (10^5) of freshly purified extracellular parasites incubated with D-luciferin (0.15 mg/ml) and coelenterazine (10 μg/ml) to measure *F-Luc* and *R-Luc* activity, respectively. n.d., not determined. (B) Expression of *F-Luc* and *R-Luc* in vivo. Mice infected with clones H3, D5, H3F33, H3E33, D5D33, and D5E33 were analyzed for *F-Luc* activity by BLI at 15 to 18 days postinfection. Mice infected with clones H3F33, H3E33, D5D33, and D5E33 were also analyzed for *R-Luc* activity at 5 days postinfection. Representative images were collected after injecting the mice i.p. with 200 μl of either coelenterazine (15 μg/ml) or D-luciferin (15 mg/ml). Brains collected at 30 days postinfection from H3F33-, H3E33-, D5D33-, and D5E33-infected animals were homogenized and analyzed by confocal fluorescence microscopy to investigate the expression of EGFP in parasite cysts. (C) Quantification of *F-Luc* specific activity in tissue cysts. Increasing numbers of intact cysts purified from the brains of H3-infected mice were analyzed for photon emission in a 24-well plate. The numbers (13, 23, or 56) and the integrity of the cysts were confirmed by optical microscopy. Under these experimental conditions, the photon activity of individual cysts ranged from 9,000 to 13,000. (D) Access of D-luciferin to tissue cyst bradyzoites, showing photon emission comparison of encysted and free bradyzoites. Either intact or trypsin-treated brain cysts were analyzed for photon emission. Infected brain showing a positive BLI signal was homogenized, resuspended in 1 ml of 1× PBS, split into two samples, and imaged for 5 min using the Xenogen IVIS200 system (first reading). One of the aliquots was treated with 0.5% trypsin (well 2) for 5 min at 37°C to release the bradyzoites from the cysts, and both samples were assayed again by BLI for 5 min (second reading). Release of bradyzoites was confirmed by optical microscopy.

of the substrates, the parasites were incubated for 5 min; thereafter, each sample was imaged for 5 min with the Xenogen IVIS system. *F-Luc* photon emission generated from bradyzoites and tissue cysts in live infected mice was revealed after injecting the animals i.p. with two consecutive doses of 200 μl of D-luciferin (150 mg substrate/kg of body weight) given at 20 min apart. Images were collected (5 min of acquisition) 30 min after the second inoculation of substrate. Total photon emission from selected anatomical regions of interest was calculated using the Living Image software and IGOR PRO 4.09A. *R-Luc* activity was detected after injecting mice with a single dose (200 μl i.p.) of coelenterazine (15 μg/ml). Images were collected from mice anesthetized with isoflurane and processed with the IVIS200 system 30 min after the administration of coelenterazine. To compare BLIs obtained at subsequent days postinfection and in different experiments, background photon emission values obtained from mice infected with wild-type parasites (control) were subtracted. The cutoff value of the photon emission background in the control mice was calculated as the number of photons/s/cm^2/sr that gave no detectable image signal. To quantify the photon emission in defined anatomical regions of interest, the selected area was defined using IGOR PRO software. To collect total flux from the brain, the width and height of the region of interest were fixed to 1.1 and 1.6 cm, respectively. The total flux collected was calculated as the function of number of photons per second captured. To analyze individual organs by BLI, mice were culled and tissues and organs were soaked for 5 min in either D-luciferin (300 μg/ml) or coelenterazine (20 μg/ml) and imaged ex vivo.

RESULTS

Development of *T. gondii* parasites expressing distinct bradyzoite and tachyzoite bioluminescent markers. To visualize tachyzoite-to-bradyzoite conversion and tissue cyst distribution in vivo, we transformed *T. gondii* parasites (PLK, a clone of strain ME49) with a construct containing the *F-Luc* gene under the transcriptional control of the bradyzoite-transcribed *SRS9* promoter (Fig. 1). Parasites expressing the luciferase gene upon differentiation into bradyzoites were selected in in vitro experiments. Individual clones growing on HFF cells were induced to switch into bradyzoites upon exposure to alkaline medium (pH 8.1). These parasites were analyzed for photon emission before and after pH induction, either in the absence or in the presence of *F-Luc*-specific substrate (D-luciferin). Two parasite clones, H3 and D5, showed the highest bioluminescence signal upon exposure to alkaline medium and were selected for further in vivo studies (Fig. 2A). The clones H3 and D5 showed a virulence phenotype in vivo that was indistinguishable from that of parental parasites (data not shown), and they were able to form typical tissue cysts (Fig. 2B).

We further engineered the two transgenic clones H3 and D5, with constructs containing the EGFP-coding sequence and the *R-Luc* gene under the control of the *SRS9* and *SAG1* promoters, respectively (Fig. 1). The resulting parasites were designed to express *F-Luc* and *R-Luc* in a mutually exclusive manner: *R-Luc* at the tachyzoite stage and *F-Luc* at the bradyzoite stage. This allowed the in vivo monitoring of tachyzoite-to-bradyzoite conversion in both directions. This experimental model exploits the high selectivity of *Renilla* and firefly lucif-

erases, which utilize two distinct substrates, coelenterazine and D-luciferin, respectively (4). These parasites were also designed to simultaneously express *F-Luc* and EGFP at the bradyzoite stage in order to assess correlations between in vivo and ex vivo photon emission data on the one hand and microscopic examination of tissue cysts on the other. We selected four clones on the basis of *R-Luc* expression in culture, two each from H3 and D5 parasite parental lines. The four selected clones (H3F33, H3E33, D5D33, and D5E33) constitutively expressed *R-Luc* in tachyzoite cultures as well as in infected mice (Fig. 2A and B). The expression of *R-Luc* at the tachyzoite stage did not delay in vitro growth, nor did it affect the 50% lethal dose compared to that of wild-type parasites (data not shown). Upon switching to bradyzoites in vitro, all four clones expressed both *F-Luc* and EGFP while downregulating the expression of *R-Luc* (Fig. 2A and B). The clone H3F33 was chosen for further investigation.

Quantification of *T. gondii* tissue cysts in vivo. Analysis of *F-Luc* photon emission in H3- and D5-infected mice from day 12 postinfection onwards revealed a marked signal in the heads of the animals (Fig. 2B), in agreement with the knowledge that the brain is the organ most affected by tissue cyst formation in this parasite-mouse model. Though the signal detected by BLI could originate from ongoing tachyzoite-to-bradyzoite conversion, its distribution, temporal appearance, and persistence did not rule out a contribution from differentiated bradyzoites within tissue cysts. This possibility would defy the notion that the cyst wall structure prevents access of complex molecules such as D-luciferin to cyst bradyzoites. We therefore investigated whether the intensity of the signal detected by BLI correlated with the number of cysts isolated from homogenized brains and assessed the ability of intact H3 and D5 tissue cysts to utilize D-luciferin in ex vivo experiments. CD1 and C57BL/6 mice were inoculated i.p. with 10^4, 10^5, and 10^6 H3 and D5 tachyzoites. These mice usually do not die during the acute phase of infection when the avirulent ME49 strain is used but instead develop a chronic disease characterized by a massive production of tissue cysts. Infected mice were monitored every day by BLI for *F-Luc* photon emission. After a period ranging between 12 and 18 days postinfection, about 80% of the mice showed a clear photon signal in the region of the head encompassing the brain (Fig. 2B) The two clones H3 and D5 showed no difference in the temporal and spatial distributions of the photon emission pattern. To identify the source of the signal, the brains were homogenized and processed by isopycnic centrifugation to search for tissue cysts. The purified cysts were analyzed for photon emission. Our results showed that the cysts purified from these brains emitted a significant amount of photons upon exposure to D-luciferin. The total flux of light emitted by the samples was directly correlated with the number of cysts, showing, at all dilutions tested, a specific activity ranging from 9,000 to 13,000 photons/s per cyst (Fig. 2C). We further assessed whether the cyst wall represented a barrier for the diffusion of D-luciferin. We compared the photon emission signals generated in vitro by intact and trypsin-treated purified tissue cysts. The trypsin treatment dissolves the cyst wall and induces the release of free bradyzoites (43). The analysis of the data revealed only a modest and not significant difference between trypsin-treated and untreated cysts (Fig. 2D). These findings indicate that D-luciferin is able to cross the wall of purified tissue cysts and argue for a role of parasite cysts as the source of photon emission detected in vivo.

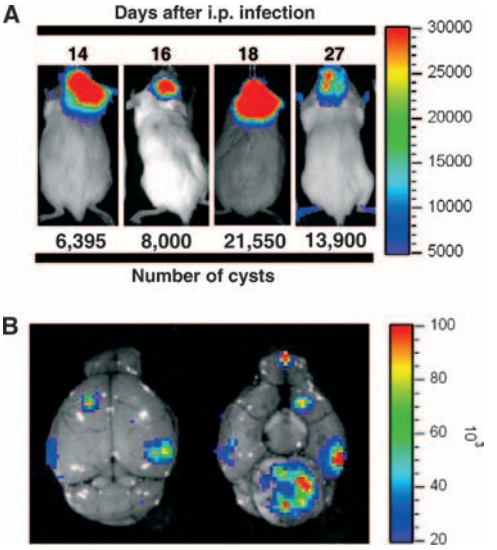

FIG. 3. (A) Correlations between BLI photon emission in vivo and cyst number recovered in the brains. The panels show photon emission images of infected CD1 mice collected shortly before the spontaneous death of the animals. The day postinfection of BLI analysis is indicated together with the number of cysts recovered from individual brains. (B) Ex vivo analysis of an infected brain, showing photon emission analysis of H3F33-infected mouse brain soaked in D-luciferin and imaged from both the top and the base for 5 min with the Xenogen IVIS200 system.

To better quantify the correlation between the imaging data and cyst formation, we purified and determined the number of cysts present in the brains of infected mice showing different level of photon emission in vivo. This analysis was performed with mice infected with H3F33 parasites. These bradyzoites also express EGFP, thus facilitating the identification of cysts in the brain homogenates. Microscopic examination revealed that at around day 18 postinfection, the brain homogenate from mice showing high photon emission contained between 6,000 and 21,000 cysts (Fig. 3A). A much lower number of cysts (between 150 to 400 per mouse) was detected in the brains of infected mice that showed no photon signal at day 30. The in vivo cyst detection limit of BLI did not depend exclusively on cyst numbers. Photon emission was also influenced by the size and the localization of the tissue cysts in the brain. Cysts localized on the surface of the hemispheres produced a higher signal in vivo than cysts localized at the base of the brain. Indeed, analysis of isolated brains incubated with D-luciferin and analyzed for photon emission revealed the presence of signals at the base of the brain that could not be detected in live animals (Fig. 3B). When the cutoff of the background signal was set at 5,000 photons/s/cm^2/sr, a level in which a BLI signal is never observed in control mice, the detection threshold limit was about 150 cysts per brain.

Kinetics of tachyzoite-to-bradyzoite conversion and cyst formation. The H3F33 parasites offer the unique opportunity to determine the distribution and the intensity of tachyzoite in-

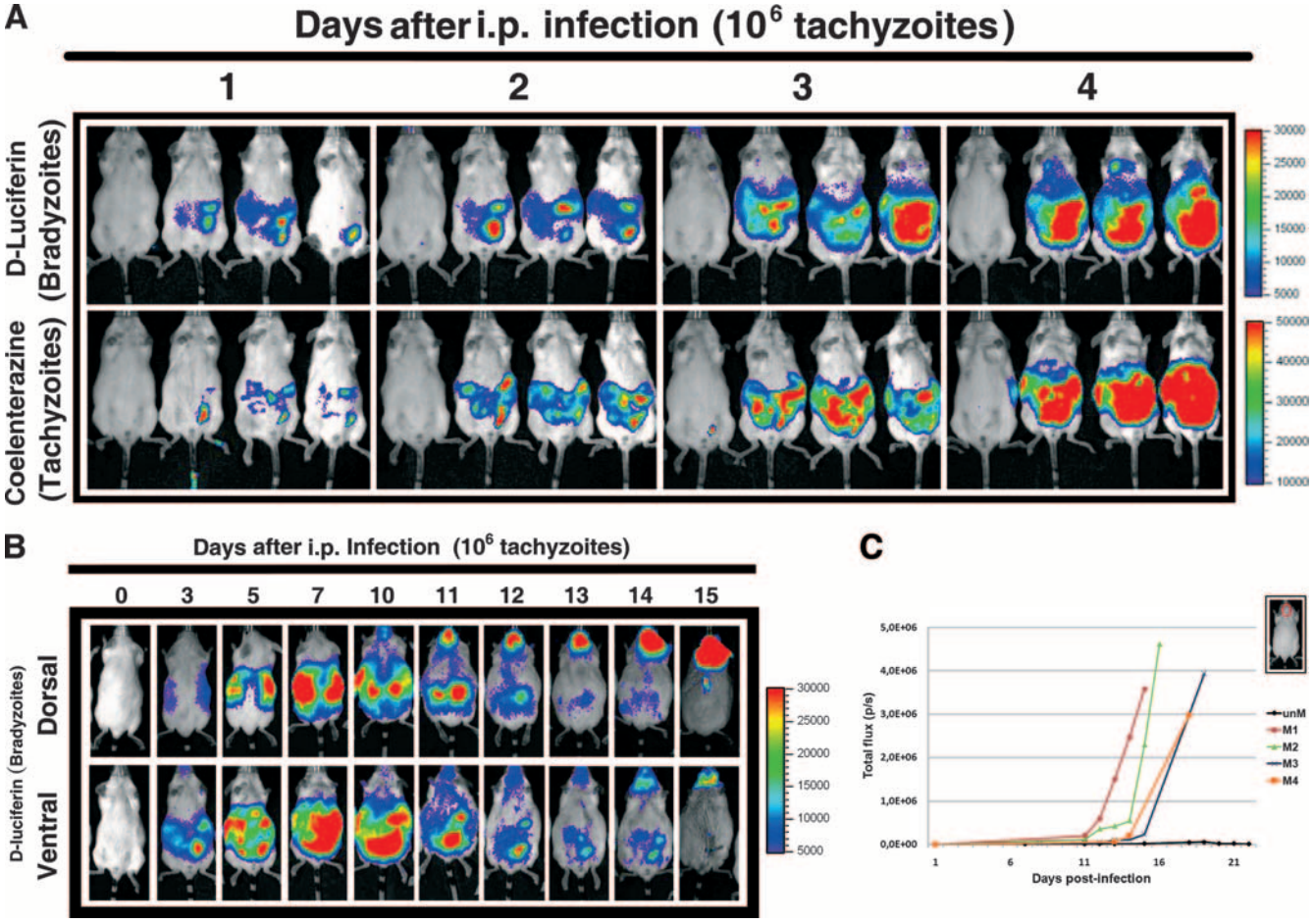

FIG. 4. Spatial and temporal distribution of luciferase activity in mice infected with a lethal parasite inoculum. (A) Monitoring of *F-Luc* and *R-Luc* activities during the early phase of *T. gondii* infection. Mice (CD1) were infected using 10^6 H3F33 tachyzoites and analyzed by BLI for four consecutive days after administration of substrates selective for bradyzoite (D-luciferin, upper row) and tachyzoite (coelenterazine, lower row) transcribed luciferase genes. The scale of the signal intensity (color bar) for *F-Luc* was set at between 5,000 and 30,000 photons/s/cm^2/sr, whereas that for *R-Luc* was set at between 10,000 and 50,000 photons/s/cm^2/sr. The experiment shown was conducted in triplicates. Uninfected animals were included to quantify the photon emission background (first mouse from the left in each panel). (B) Animals infected i.p. with 10^6 H3F33 tachyzoites were analyzed daily for photon emission to monitor bradyzoite formation. The panels show dorsal and ventral BLI analysis of a representative mouse. In this mouse the number of brain cysts determined microscopically after death at day 16 postinfection was about 21,500. The scale of the signal intensity (color bar) is included. (C) Time course of *F-Luc* photon emission activity from individual mice infected with 10^6 H3F33 tachyzoites (color coded M1 to M4). Photon emission counts (p/s) were collected daily over a period of 40 days from an area of the head (region of interest) encompassing the brain (inset). As a control, photon emission values were collected from the same region of interest of uninfected mice (unM).

fection as well as tachyzoite-to-bradyzoite conversion in the same mouse. We monitored daily the photon emission in H3F33-infected CD1 mice starting from the day of the inoculation. Infected mice were injected first with D-luciferin to detect *F-Luc* photon emission (generated by the bradyzoites), and then after 4 h (when the BLI signal was no longer detectable), the same mice were injected with coelenterazine to detect *R-Luc* tachyzoite activity. As early as day 1 postinfection, mice inoculated with 10^6 H3F33 tachyzoites showed a high *F-Luc* activity, suggesting a massive conversion from tachyzoites to bradyzoites (Fig. 4A). In these mice the *F-Luc* signal was confined to the abdomen and could be superimposed on the photon image generated on the same day by *R-Luc* (tachyzoites). At day 4, *F-Luc* and *R-Luc* photon emissions reached the highest intensity, and infected mice usually died shortly afterwards. Few mice survived and cleared the acute tachyzoite infection. These surviving animals showed a high BLI signal in the brain only later, at about 14 to 18 days postinfection, and died a few days later (Fig. 4B and C). Mice injected with a lower number of H3F33 parasites (10^5) showed a peak of *F-Luc* activity in the abdomen at around day 7 postinfection, which disappeared a few days later (Fig. 5A). In these mice *F-Luc* photon emission appeared again at around day 12 postinfection, when it was localized exclusively in the head. Photon emission showed a steady increase in the following 7 days and then decreased to the point that no signal was detectable at around day 30 postinfection (Fig. 5A). Figure 5B shows the kinetics of tissue cyst formation in the brains of several mice infected with 10^5 H3F33 tachyzoites. To identify the organs and tissues involved in this unexpected and early tachyzoite-to-bradyzoite conversion, CD1 mice were infected with 10^5 H3F33 tachyzoites and culled at day 5 postinfection,

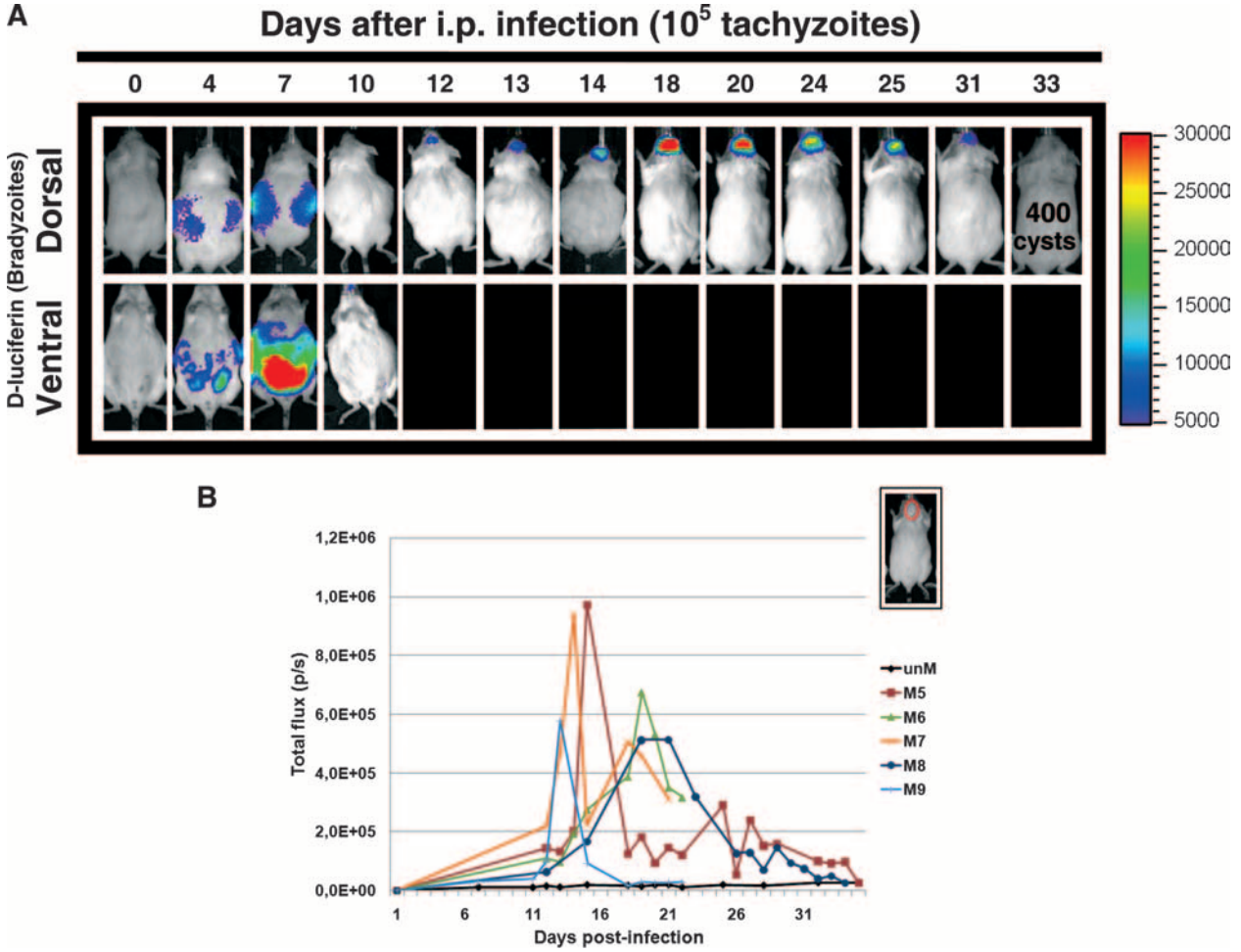

FIG. 5. Spatial and temporal distributions of *F-Luc* activity in animals developing chronic infection. (A) Animals infected i.p. with 10^5 H3F33 tachyzoites were analyzed daily for photon emission to monitor bradyzoite formation. The panels show dorsal and ventral BLI analysis of a representative mouse. At day 33 postinfection, when the BLI signal had disappeared, the animal was culled and the number of cysts present in the brain was determined by fluorescence microscopic examination. The signal intensity scale (color bar) is included. (B) Time course of *F-Luc* photon emission activity from individual mice (color coded M5 to M9) infected with 10^5 H3F33 tachyzoites. Photon emission counts (p/s) were collected daily over a period of 40 days from an area of the head (region of interest) encompassing the brain (inset).

when *F-Luc* photon emission was still high. The abdomens of the animals were exposed and analyzed for *F-Luc* and *R-Luc* photon emission to localize the source of the signal. We observed that both *F-Luc* and *R-Luc* activity localized in the same regions, particularly in the adipose tissue surrounding the stomach, intestine, and liver (Fig. 6A and B). Confocal fluorescence microscopy analysis of the dissected adipose tissue showed a high number of fluorescent isolated bradyzoites (Fig. 6C). Notably, we never observed the presence of tissue cysts at this stage. Expression of other bradyzoite-specific genes, i.e., *BAG1*, *ENO1*, *LDH2*, and *PMA1*, was detected by RT-PCR in H3F33 parasites purified from the peritoneal cavities of mice at 4 days postinfection (Fig. 6D). These bradyzoite markers were not detected in the H3F33 tachyzoites cultured in vitro and used for the i.p. infections (Fig. 6D). *ENO2* and *LDH1*, which are specifically transcribed only in the tachyzoite stage, were detected in both samples, as expected since most parasites growing in the peritoneal cavity are tachyzoites. These results indicated that the *F-Luc* activity detected at this stage is part of a more general induction of bradyzoite-specific promoters.

We also studied the kinetics of cyst formation after oral infection in CD1 mice. These experiments showed that oral infection usually resulted in a longer time for cyst formation in the brain, as inferred by *F-Luc* photon emission pattern (Fig. 7). Moreover, the signal rarely reached the high values observed with i.p. injection. In orally infected animals cyst formation showed a major peak that appeared slightly delayed compared to that with i.p. infection, at around day 14 to 28 postinfection, followed by several peaks of decreasing intensity until no signal was detectable.

Localization and distribution of tissue cysts in the nervous central system. A number of CD1 and C57BL/6 mice infected with 10^5 H3F33 tachyzoites showing *F-Luc* photon emission were culled for the purpose of investigating cyst density and distribution in intact brains. This analysis showed that rather than being equally distributed in the brain, photon emission was localized in intense small clusters. Spots of signal were

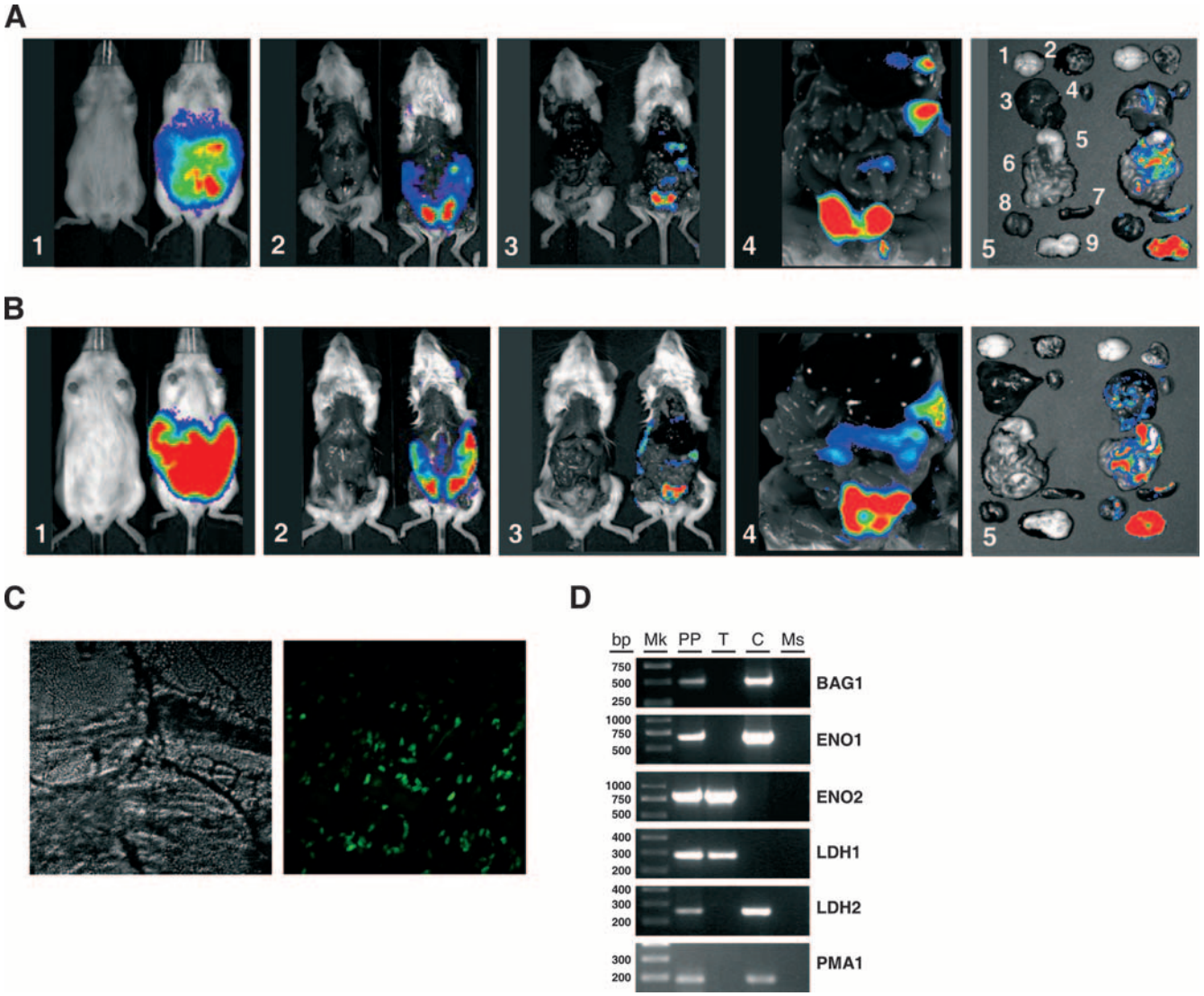

FIG. 6. Distribution of *F-Luc* and *R-Luc* activities in organ and tissues. CD1 mice infected with 10^5 H3F33 tachyzoites were culled at day 5 postinfection for BLI analysis of internal organs. Uninfected (left) and H3F33-infected (right) mice were analyzed in parallel. Live mice were injected i.p. with 200 μl of either D-luciferin (A) or coelenterazine (B) to detect *F-Luc* and *R-Luc* activity, respectively, and imaged for 5 min with the Xenogen IVIS200 system. After in vivo imaging (1), mice were culled for ex vivo analysis: the fur coat was removed from the abdomen, leaving internal organs at their original positions still included into the peritoneal membrane (2); the peritoneal membrane was removed to expose internal organs and tissues (3); the bare abdomens of infected mice were analyzed (4); and individual organs were removed and analyzed for photon emission (5). In each photograph the background setting was set independently to better visualize the BLI signal. The organs shown, from the top to the bottom, are as follows: 1, brain; 2, lung; 3, liver; 4, heart; 5, stomach; 6, intestine; 7, spleen; 8, kidney; 9, fat body. (C) The adipose tissue dissected from an infected mouse was spread over a slide and analyzed by confocal fluorescence microscopy. Fluorescent bradyzoites but no cysts were found all over the tissue. Photomicrographs show transmission and fluorescence images. (D) Expression of bradyzoite markers in early days of infection with H3F33 parasites. The panels show RT-PCRs of *BAG1*, *ENO1*, *ENO2*, *LDH1*, *LDH2*, and *PMA1*. The first lane contains the 1-kb DNA ladder (Mk), and the successive lanes are loaded with the products of RT-PCRs performed on the total RNA extracted from the following samples: H3F33 parasites recovered from the peritoneal cavities of mice at 4 days postinfection (PP), H3F33 tachyzoites grown in in vitro cultures of HFF cells (T), purified cysts from brains of mice infected with H3F33 (C), and brain from an uninfected mouse (Ms).

found in the cerebral cortex, superior and inferior colliculus, cerebellum, olfactory bulbs, and medulla oblongata (Fig. 8A). To better characterize the source of the signal, a portion of cerebral tissue showing a single focus of photon emission was removed from the brain by thin sectioning (Fig. 8B) and analyzed by optical fluorescence microscopy. Our results showed that individual photon emission foci are generated by a number of tissue cysts closely clustered together (Fig. 8C). Figure 8B shows a representative example in which 60 cysts were counted in a piece of cerebral tissue, corresponding to a focus of BLI signal. We also searched for the presence of tachyzoites in the brains of chronically infected mice showing strong *F-Luc* photon emission. After *F-Luc* photon emission induced by D-luciferin was no longer detectable, mice were injected i.p. with coelenterazine and analyzed by BLI. Since no signal was detected in any region of the body, the mice were culled and

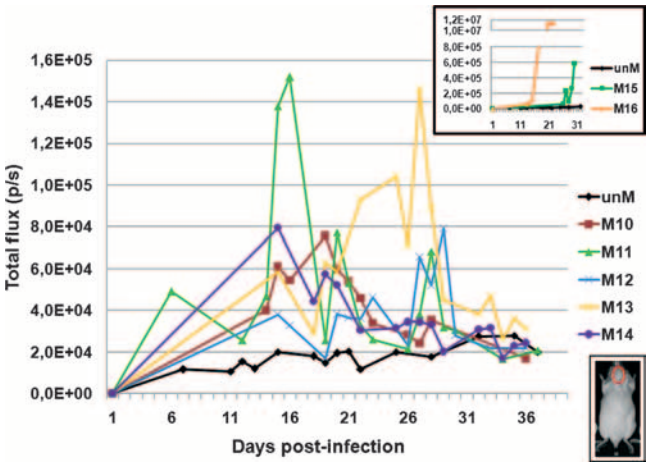

FIG. 7. Time course of *F-Luc* activity in the heads of individual animals infected by oral gavage of H3F33 cysts. CD1 mice (color coded M10 to M16) were infected by oral administration of a brain homogenate containing about 200 cysts of H3F33 parasites. Photon emission counts (p/s) were collected over a period of 40 days from an area of the mouse head (region of interest) encompassing the brain (bottom inset). Photon emission counts collected from the same region of interest of uninfected mice (unM) were also assessed in each BLI assay. The top inset shows on a different scale the photon emission of the cerebral areas of those mice that showed high BLI signals.

the brains were harvested for further investigation. BLI analysis of the dissected brains with coelenterazine showed low but detectable levels of *R-Luc* activity, thus revealing the presence of tachyzoites in the brains of infected mice at this stage of the infection (data not shown). To investigate whether cyst formation was restricted to brain or whether it occurred also in other sites of the central nervous system, the spinal cord was dissected from infected mice that showed a BLI signal in the head and this was analyzed for the presence of cysts. As shown in Fig. 8D, photon emission was detected along the spinal cord, and confocal microscopy confirmed that the signal was due to the presence of mature cysts inside the spinal cord (Fig. 8E).

DISCUSSION

We have engineered the *T. gondii* strain ME49 to express *R-Luc* and *F-Luc* in a mutually exclusive manner at the tachyzoite and bradyzoite stages, respectively. Phenotypic analysis confirmed that the clones H3F33, H3E33, D5D33, and D5E33 constitutively expressed *R-Luc* during propagation in culture at the tachyzoite stage. Upon exposure to alkaline pH, a condition known to induce differentiation into bradyzoites, the parasites downregulated the production of *R-Luc* while inducing the synthesis of *F-Luc*. The selectivity of *R-Luc* and *F-Luc* for different substrates allowed us to study in vivo both tachyzoite dissemination and tachyzoite-to-bradyzoite conversion. Monitoring by BLI of mice infected with H3F33 revealed that during the first days postinfection, *R-Luc* photon emission was localized mainly in the abdomen. This pattern is similar to that previously observed when mice were infected with tachyzoites expressing firefly luciferase (8, 10, 20, 36). Autopsies carried out shortly after BLI analysis revealed that the signal was localized to the adipose tissue surrounding the ab-

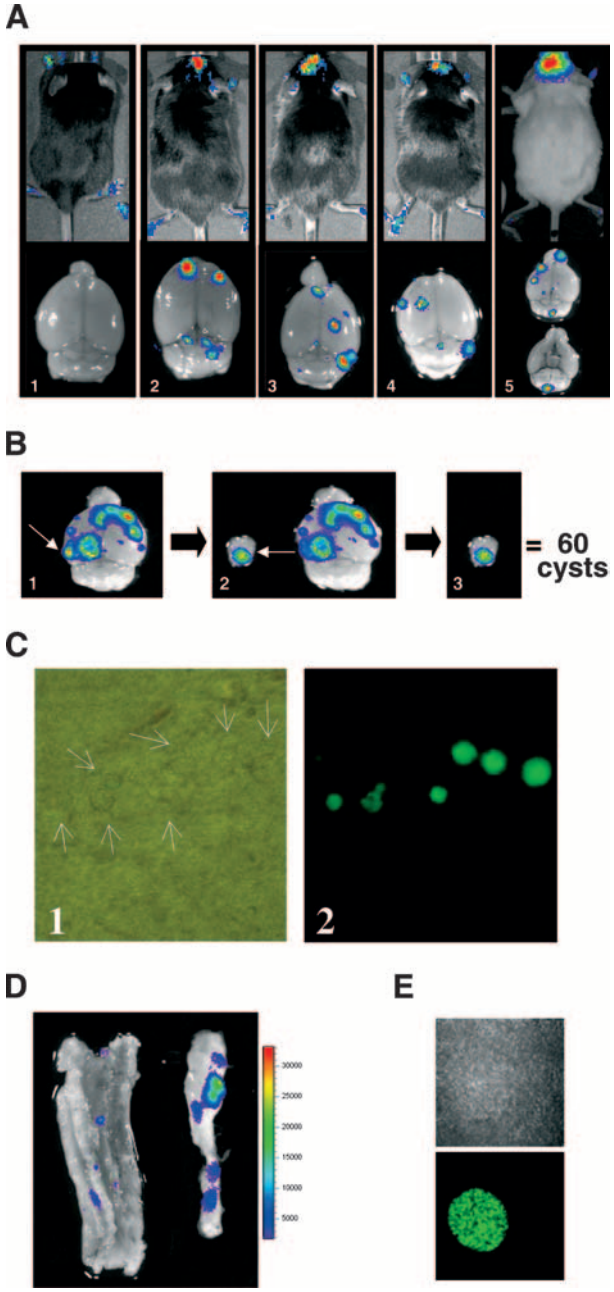

FIG. 8. Analysis of cyst distribution in the central nervous system of H3F33-infected mice. (A) C57BL/6 (black fur) and CD1 (white fur) mice were injected i.p. with D-luciferin at around day 16 postinfection and in vivo imaged. Brains from these mice were collected shortly afterwards and analyzed by BLI to investigate the correlation between in vivo and ex vivo signals (1 to 5). (B) Determination of cyst number from individual photon emission foci. H3F33 infected mice were culled at day 18 postinfection to analyze their brains by BLI. Images were acquired for 5 min after soaking the brain in a solution containing D-luciferin (300 μg/ml in PBS) (1). Portions of brain containing isolated foci of photon emission were dissected (2 and 3), spread over a microscope slide, and analyzed by fluorescence microscopy to determine the total amount of cysts. The dissected focus contained 60 cysts. (C) Transmission (1) and fluorescence (2) photomicrographs of a brain section showing the distribution of cysts expressing EGFP. (D) BLI analysis (5 min of photon collection) of dissected spinal cords from H3F33 infected mice soaked in D-luciferin (300 μg/ml in PBS) for 5 min. (E) Spinal cords displaying a BLI signal were spread on microscope slides and analyzed by fluorescence microscopy. Mature cysts were found in this tissue. The pictures show transmission and fluorescence images.

dominal organs. Unexpectedly, in these animals we also observed a strong *F-Luc* signal that was spatially superimposed on that of *R-Luc*. The intensity and the temporal expression of *F-Luc* photon emission varied with the number of parasites injected. Mice inoculated with 10^6 parasites showed a high level of signal as early as day 1 postinfection that lasted for 5 to 12 days and disappeared thereafter in the surviving animals. When 10^5 parasites were injected, the *F-Luc* photon emission was detected at around day 4 postinfection and lasted 2 to 5 days. We interpreted these results as evidence of massive tachyzoite-to-bradyzoite conversion coinciding with initial tachyzoite dissemination. Microscopic analysis of tissues and organs examined shortly after BLI analysis confirmed this hypothesis. The adipose tissue had a high number of individual bradyzoites identified on the basis of EGFP expression, which, in H3F33, coincides with the *F-Luc* expression pattern since both genes are under the transcriptional control of the *SRS9* bradyzoite promoter.

Ectopic expression of the *SRS9* promoter due to a positional effect was thus ruled out by the observation that the EGFP expression always coincided with *F-Luc* activity. We also attempted to reproduce the results obtained with the *SRS9* promoter by generating parasites expressing either *F-Luc* or EGFP under the transcriptional control of the bradyzoite-specific *BAG1* promoter. These parasites showed an *F-Luc* activity profile in vivo that was superimposed on that observed when using the H3F33 parasites, including the early peak of activity detected in the initial phase of infection (data not shown).

Examinations carried out on subsequent days revealed that this massive tachyzoite-to-bradyzoite switch in the early phase of infection was not followed by cyst formation. Mice that survived the acute phase of infection showed a sharp decrease of *F-Luc* photon emission in the abdomen. Microscopy analysis indicated that the bradyzoites had disappeared from the adipose tissue. These findings shed new light onto the process of tachyzoite-to-bradyzoite conversion and cyst formation. Contrary to common knowledge, *Toxoplasma* finds in vivo the conditions that trigger the differentiation into bradyzoites very early during the infection, although this conversion might be only partial and bradyzoites may reverse back to tachyzoites before complete differentiation, thus explaining why we did not find cysts in the adipose tissue. Furthermore, in this experimental model the differentiation into bradyzoites observed in the adipose tissue was not followed by cyst formation, thus indicating that though the two processes are intimately linked, the latter process can be arrested or aborted. In addition, the *F-Luc* expression pattern in the absence of cyst formation may reflect the occurrence of a generalized tachyzoite-to-bradyzoite interconversion process that takes place early during infection to eliminate those parasites that, once differentiated into bradyzoites, have lost the ability to differentiate back into tachyzoites as they would not be infective.

Parasites expressing *F-Luc* under the transcriptional control of the *SRS9* promoter also proved invaluable in assessing cyst formation in vivo in those mice that survived the acute phase of infection. Our results demonstrated that there was a linear correlation between *F-Luc* photon emission generated in the heads of infected mice and cyst numbers detected microscopically in the brains of infected animals examined shortly after BLI analysis. Furthermore, trypsin treatment of brain cysts did not result in a noticeable increase in the *F-Luc* signal. These findings strongly argue that D-luciferin has access to bradyzoites within intact cysts both in vitro and in vivo, a finding which suggests a revision of the idea that *Toxoplasma* is protected from the attack of most drugs at this developmental stage. Monitoring of cyst formation in vivo showed that the brain is the main organ involved. BLI analysis of H3- or H3F33-infected animals showed that *F-Luc* photon emission was localized mainly in the heads of the mice. The pattern of cyst formation, also confirmed by microscopic examination, was characterized by a first phase of cyst development at around days 12 to 16 postinfection, followed by a sharp decrease in their numbers. In the animals that were initially inoculated with a lower dose of parasites, we observed subsequent waves of cyst expansion and reduction. This pattern of cyst formation was particularly evident with oral infections.

The sharp reduction of *F-Luc* photon emission observed in the brain, as well as microscopic analysis, indicated that most of the early cysts are lost during the first weeks of infection. In some mice we observed a spontaneous reduction in the cyst number from about 20,000 to less than 200, the number of cysts that produced a bioluminescence signal that is no longer detectable in vivo by the IVIS200 system. This limit of sensitivity may explain why cysts in skeletal muscles were not detected using BLI, since the density of cysts in this tissue is likely to be below the threshold of detection that we set.

In addition, the focal distribution of cysts would indicate that they are generated by very few parasite precursors. Apparently not all cell types in the brain can equally support the growth of *Toxoplasma* cysts. Access to nutrients and exposure to immune effectors may operate a dramatic selection process. Notably, the few surviving cysts, irrespective of the time postinfection or their size, are still transcriptionally active as inferred by *F-Luc* activity and EGPF expression and, most importantly, remain permeable to D-luciferin. The development of *T. gondii* parasites expressing a bioluminescent marker at the bradyzoite stage not only unravels, for the first time, unanticipated clues about tachyzoite-to-bradyzoite conversion and cyst formation in vivo but also indicates that cysts are accessible to complex molecules such as D-luciferin, thus providing both a case for testing drugs targeting this parasite developmental stage and a suitable readout system.

ACKNOWLEDGMENTS

We thank Francesco Bistoni and Tania Dottorini for helpful discussions. We thank the Malaria Research and Reference Reagent Resource Center for providing us with plasmid pL0028, contributed by Andrew P. Waters. We also thank Tony Nolan for linguistic revision of the manuscript.

This work was supported by grants from the Italian Ministry of Research PRIN (Research Programme for Relevant National Interest, grant 2005065913_005) and FIRB (Basic Research Investments Programme, grant RBLA03C9F4_001).

REFERENCES

1. **Araujo, F. G., J. Huskinson, and J. S. Remington.** 1991. Remarkable in vitro and in vivo activities of the hydroxynaphthoquinone 566C80 against tachyzoites and tissue cysts of *Toxoplasma gondii*. Antimicrob. Agents Chemother. **35:**293–299.
2. **Araujo, F. G., J. Huskinson-Mark, W. E. Gutteridge, and J. S. Remington.** 1992. In vitro and in vivo activities of the hydroxynaphthoquinone 566C80 against the cyst form of *Toxoplasma gondii*. Antimicrob. Agents Chemother. **36:**326–330.

3. **Barcan, L. A., M. L. Dallurzo, L. O. Clara, A. Valledor, S. Macias, E. Zorkin, S. Gerona, and B. Livellara.** 2002. *Toxoplasma gondii* pneumonia in liver transplantation: survival after a severe case of reactivation. Transpl. Infect. Dis. **4:**93–96.
4. **Bhaumik, S., and S. S. Gambhir.** 2002. Optical imaging of Renilla luciferase reporter gene expression in living mice. Proc. Natl. Acad. Sci. USA **99:**377–382.
5. **Black, M., F. Seeber, D. Soldati, K. Kim, and J. C. Boothroyd.** 1995. Restriction enzyme-mediated integration elevates transformation frequency and enables co-transfection of *Toxoplasma gondii*. Mol. Biochem. Parasitol. **74:**55–63.
6. **Bohne, W., J. Heesemann, and U. Gross.** 1993. Induction of bradyzoite-specific *Toxoplasma gondii* antigens in gamma interferon-treated mouse macrophages. Infect. Immun. **61:**1141–1145.
7. **Bohne, W., J. Heesemann, and U. Gross.** 1994. Reduced replication of *Toxoplasma gondii* is necessary for induction of bradyzoite-specific antigens: a possible role for nitric oxide in triggering stage conversion. Infect. Immun. **62:**1761–1767.
8. **Boyle, J. P., J. P. Saeij, and J. C. Boothroyd.** 2007. *Toxoplasma gondii*: inconsistent dissemination patterns following oral infection in mice. Exp. Parasitol. **116:**302–305.
9. **Cornelissen, A. W., J. P. Overdulve, and J. M. Hoenderboom.** 1981. Separation of *Isospora* (*Toxoplasma*) *gondii* cysts and cystozoites from mouse brain tissue by continuous density-gradient centrifugation. Parasitology **83:** 103–108.
10. **Dellacasa-Lindberg, I., N. Hitziger, and A. Barragan.** 2007. Localized recrudescence of *Toxoplasma* infections in the central nervous system of immunocompromised mice assessed by *in vivo* bioluminescence imaging. Microbes Infect. **9:**1291–1298.
11. **Dubey, J. P., D. S. Lindsay, and C. A. Speer.** 1998. Structures of *Toxoplasma gondii* tachyzoites, bradyzoites, and sporozoites and biology and development of tissue cysts. Clin. Microbiol. Rev. **11:**267–299.
12. **Eaton, M. S., L. M. Weiss, and K. Kim.** 2006. Cyclic nucleotide kinases and tachyzoite-bradyzoite transition in *Toxoplasma gondii*. Int. J. Parasitol. **36:** 107–114.
13. **Ferguson, D. J., J. Huskinson-Mark, F. G. Araujo, and J. S. Remington.** 1994. An ultrastructural study of the effect of treatment with atovaquone in brains of mice chronically infected with the ME49 strain of *Toxoplasma gondii*. Int. J. Exp. Pathol. **75:**111–116.
14. **Ferguson, D. J., W. M. Hutchison, and E. Pettersen.** 1989. Tissue cyst rupture in mice chronically infected with *Toxoplasma gondii*. An immunocytochemical and ultrastructural study. Parasitol. Res. **75:**599–603.
15. **Frenkel, J. K., and A. Escajadillo.** 1987. Cyst rupture as a pathogenic mechanism of toxoplasmic encephalitis. Am. J. Trop. Med. Hyg. **36:**517–522.
16. **Frenkel, J. K., B. M. Nelson, and J. Arias-Stella.** 1975. Immunosuppression and toxoplasmic encephalitis: clinical and experimental aspects. Hum. Pathol. **6:**97–111.
17. **Gormley, P. D., C. E. Pavesio, D. Minnasian, and S. Lightman.** 1998. Effects of drug therapy on *Toxoplasma* cysts in an animal model of acute and chronic disease. Investig. Ophthalmol. Vis. Sci. **39:**1171–1175.
18. **Grosu, I., O. Ghekiere, N. Layios, P. Hantson, and G. Cosnard.** 2007. *Toxoplasma* encephalitis after autologous stem cell transplantation. Leukoc. Lymphoma **48:**201–203.
19. **Haverkos, H. W., et al.** 1987. Assessment of therapy for *Toxoplasma* encephalitis. Am. J. Med. **82:**907–914.
20. **Hitziger, N., I. Dellacasa, B. Albiger, and A. Barragan.** 2005. Dissemination of *Toxoplasma gondii* to immunoprivileged organs and role of Toll/interleukin-1 receptor signalling for host resistance assessed by *in vivo* bioluminescence imaging. Cell. Microbiol. **7:**837–848.
21. **Hofflin, J. M., F. K. Conley, and J. S. Remington.** 1987. Murine model of intracerebral toxoplasmosis. J. Infect. Dis. **155:**550–557.
22. **Hommann, M., U. Schotte, R. Voigt, H. Glutig, T. Grube, B. Kupper, A. Kornberg, K. Richter, and J. Scheele.** 2002. Cerebral toxoplasmosis after combined liver-pancreas-kidney and liver-pancreas transplantation. Transplant Proc. **34:**2294–2295.
23. **Kim, K., D. Soldati, and J. C. Boothroyd.** 1993. Gene replacement in *Toxoplasma gondii* with chloramphenicol acetyltransferase as selectable marker. Science **262:**911–914.
24. **Kirkman, L. A., L. M. Weiss, and K. Kim.** 2001. Cyclic nucleotide signaling in *Toxoplasma gondii* bradyzoite differentiation. Infect. Immun. **69:**148–153.
25. **Kovacs, J. A., et al.** 1992. Efficacy of atovaquone in treatment of toxoplasmosis in patients with AIDS. Lancet **340:**637–638.
26. **Leport, C., F. Raffi, S. Matheron, C. Katlama, B. Regnier, A. G. Saimot, C. Marche, C. Vedrenne, and J. L. Vilde.** 1988. Treatment of central nervous system toxoplasmosis with pyrimethamine/sulfadiazine combination in 35 patients with the acquired immunodeficiency syndrome. Efficacy of long-term continuous therapy. Am. J. Med. **84:**94–100.
27. **Lopez-Duarte, M., A. Insunza, E. Conde, A. Iriondo, F. Mazorra, and A. Zubizarreta.** 2003. Cerebral toxoplasmosis after autologous peripheral blood stem cell transplantation. Eur. J. Clin. Microbiol. Infect. Dis. **22:**548–550.
28. **Luft, B. J., R. G. Brooks, F. K. Conley, R. E. McCabe, and J. S. Remington.** 1984. Toxoplasmic encephalitis in patients with acquired immune deficiency syndrome. JAMA **252:**913–917.
29. **Luft, B. J., R. Hafner, A. H. Korzun, C. Leport, D. Antoniskis, E. M. Bosler, D. D. Bourland III, R. Uttamchandani, J. Fuhrer, J. Jacobson, et al.** 1993. Toxoplasmic encephalitis in patients with the acquired immunodeficiency syndrome. N. Engl. J. Med. **329:**995–1000.
30. **Luft, B. J., and J. S. Remington.** 1992. Toxoplasmic encephalitis in AIDS. Clin. Infect. Dis. **15:**211–222.
31. **Lyons, R. E., R. McLeod, and C. W. Roberts.** 2002. *Toxoplasma gondii* tachyzoite-bradyzoite interconversion. Trends Parasitol. **18:**198–201.
32. **Ortonne, N., P. Ribaud, V. Meignin, C. Sarfati, H. Esperou, A. Devergie, E. Gluckman, G. Socie, and A. Janin.** 2001. Toxoplasmic pneumonitis leading to fatal acute respiratory distress syndrome after engraftment in three bone marrow transplant recipients. Transplantation **72:**1838–1840.
33. **Parmley, S. F., S. Yang, G. Harth, L. D. Sibley, A. Sucharczuk, and J. S. Remington.** 1994. Molecular characterization of a 65-kilodalton *Toxoplasma gondii* antigen expressed abundantly in the matrix of tissue cysts. Mol. Biochem. Parasitol. **66:**283–296.
34. **Remington, J. S., and R. McLeod.** 1988. Toxoplasmosis, p. 1620–1640. *In* S. L. Gorbach, J. G. Bartlett, and N. R. Blacklow (ed.), Infectious diseases, 2nd ed. W. B. Saunders, Philadelphia, PA.
35. **Roos, D. S., R. G. Donald, N. S. Morrissette, and A. L. Moulton.** 1994. Molecular tools for genetic dissection of the protozoan parasite *Toxoplasma gondii*. Methods Cell Biol. **45:**27–63.
36. **Saeij, J. P., J. P. Boyle, M. E. Grigg, G. Arrizabalaga, and J. C. Boothroyd.** 2005. Bioluminescence imaging of *Toxoplasma gondii* infection in living mice reveals dramatic differences between strains. Infect. Immun. **73:**695–702.
37. **Silva, N. M., W. L. Tafuri, J. I. Alvarez-Leite, J. R. Mineo, and R. T. Gazzinelli.** 2002. *Toxoplasma gondii*: in vivo expression of BAG-5 and cyst formation is independent of TNF p55 receptor and inducible nitric oxide synthase functions. Microbes Infect. **4:**261–270.
38. **Soete, M., and J. F. Dubremetz.** 1996. *Toxoplasma gondii*: kinetics of stage-specific protein expression during tachyzoite-bradyzoite conversion *in vitro*. Curr. Top. Microbiol. Immunol. **219:**76–80.
39. **Soete, M., B. Fortier, D. Camus, and J. F. Dubremetz.** 1993. *Toxoplasma gondii*: kinetics of bradyzoite-tachyzoite interconversion *in vitro*. Exp. Parasitol. **76:**259–264.
40. **Soldati, D., and J. C. Boothroyd.** 1993. Transient transfection and expression in the obligate intracellular parasite *Toxoplasma gondii*. Science **260:**349–352.
41. **Soldati, D., K. Kim, J. Kampmeier, J. F. Dubremetz, and J. C. Boothroyd.** 1995. Complementation of a Toxoplasma gondii ROP1 knock-out mutant using phleomycin selection. Mol. Biochem. Parasitol. **74:**87–97.
42. **Tenant-Flowers, M., M. J. Boyle, D. Carey, D. J. Marriott, J. L. Harkness, R. Penny, and D. A. Cooper.** 1991. Sulphadiazine desensitization in patients with AIDS and cerebral toxoplasmosis. AIDS **5:**311–315.
43. **Tomavo, S., B. Fortier, M. Soete, C. Ansel, D. Camus, and J. F. Dubremetz.** 1991. Characterization of bradyzoite-specific antigens of *Toxoplasma gondii*. Infect. Immun. **59:**3750–3753.
44. **Torres, R. A., W. Weinberg, J. Stansell, G. Leoung, J. Kovacs, M. Rogers, J. Scott, et al.** 1997. Atovaquone for salvage treatment and suppression of toxoplasmic encephalitis in patients with AIDS. Clin. Infect. Dis. **24:**422–429.
45. **Valar, C., E. Keitel, R. L. Dal Pra, D. Gnatta, A. F. Santos, P. D. Bianco, T. C. Sukiennik, K. L. Pegas, A. E. Bittar, K. T. Oliveira, and V. D. Garcia.** 2007. Parasitic infection in renal transplant recipients. Transplant Proc. **39:**460–462.
46. **Weiss, L. M., and K. Kim.** 2000. The development and biology of bradyzoites of *Toxoplasma gondii*. Front. Biosci. **5:**D391–D405.
47. **Weiss, L. M., D. Laplace, P. M. Takvorian, H. B. Tanowitz, A. Cali, and M. Wittner.** 1995. A cell culture system for study of the development of *Toxoplasma gondii* bradyzoites. J. Eukaryot. Microbiol. **42:**150–157.
48. **Weiss, L. M., D. LaPlace, H. B. Tanowitz, and M. Wittner.** 1992. Identification of *Toxoplasma gondii* bradyzoite-specific monoclonal antibodies. J. Infect. Dis. **166:**213–215.
49. **Wong, S. Y., and J. S. Remington.** 1993. Biology of *Toxoplasma gondii*. AIDS **7:**299–316.

Editor: W. A. Petri, Jr.